RSC Advances

PAPER

View Article Online
View Journal | View Issue

Cite this: *RSC Adv.*, 2022, **12**, 31786

Evidence of a reversible redox reaction in a liquid-electrolyte-type fluoride-ion battery†

Ritsuko Yaokawa,* Tohru Shiga, Shinya Moribe and Kazuhiko Mukai

Fluoride-ion batteries (FIBs) have received significant attention as promising alternatives to conventional lithium-ion batteries, but a reversible redox reaction has not been confirmed yet for liquid-electrolyte-type FIBs. We conducted *ex situ* X-ray diffraction and energy dispersive X-ray analyses for a conventional full-cell assembly of FIBs, in which BiF_3, a Pb plate (or Pb powder), and tetraethylammonium fluoride dissolved in propylene carbonate were used as the positive electrode, negative electrode, and liquid electrolyte, respectively. A FIB using a Pb plate exhibited a flat operating voltage at ~0.29 V during the discharge reaction with a discharge capacity of ~105 mA h g^{-1}. The reversible electrochemical reaction was, however, attained when the discharge and charge capacities were controlled to be less than 20 mA h g^{-1}. In a such capacity-limited cycle test, Bi and PbF_2 phases were formed during the discharge reaction, while BiF_3 and Pb phases were generated during the charge reaction. Therefore, a reversible movement of F^- ions between the BiF_3 and Pb electrodes, *i.e.*, reversible redox reaction was firstly confirmed for the liquid-electrolyte-type FIB. We also attempted to improve the reversibility at the first cycle by replacing the Pb plate with Pb powder electrodes, and consequently, the FIB using an annealed Pb powder indicated the best electrochemical performance.

Received 12th September 2022
Accepted 28th October 2022

DOI: 10.1039/d2ra05753k

rsc.li/rsc-advances

Introduction

Lithium-ion batteries (LIBs) are based on a reversible reaction wherein Li^+ ions move back and forth between positive and negative electrodes while maintaining each core structure, *i.e.*, a topotactic reaction.[1] This topotactic reaction enables LIBs to cycle more than several thousand times but restricts their maximum volumetric energy density ($W_{vol} \cong 1000$ W h L^{-1}), hindering their widespread application, particularly in devices requiring a high energy density, such as stationary energy storage systems.[2] Recently, fluoride-ion batteries (FIBs) have received considerable attention for moving beyond LIBs because the W_{vol} of FIBs has been reported to reach ~5000 W h L^{-1} owing to their wide operating voltage (>5 V) and multivalent redox reactions.[3–7]

Despite these high expectations, many issues must be overcome to realize practical FIBs. Solid-state F^- conductors are employed as the electrolyte rather than liquid solutions to avoid the difficulties involved in preparing liquid electrolytes and to stabilize the redox reactions.[8–13] In recent years, solid electrolytes with high ionic conductivity have improved the room-temperature performance of solid-state FIBs,[11–15] but all-solid-state FIBs usually require high operating temperatures above 150 °C,[8–10] resulting in several drawbacks, *e.g.*, high cost and limited use. Many researchers have thus endeavored to replace solid electrolytes with liquid ones.[16–26] Most of these studies evaluated redox reactions in a half-cell with respect to a certain reference electrode.

To our best knowledge, only two studies on a beaker-type full-cell consisting of both positive and negative electrodes have been made by Abe and co-workers.[16,17] The first study is based on a Bi|MPPF + TMPA-TFSA|PbF_2-deposited Pb cell, where MPPF and TMPA-TFSA represent 1-methyl-1-propylpiperidinium fluoride and *N*,*N*,*N*-trimethyl-*N*-propylammonium bis(trifluoromethanesulfonyl)amide, respectively.[16] Approximately 0.3 and 0.17 mA h of charge and discharge capacities (Q_{cha} and Q_{dis}) are obtained at 25 °C, but there is no information about gravimetric Q_{cha} and Q_{dis}.[16] The gravimetric values of $Q_{cha} \cong 190$ mA h g^{-1} and $Q_{dis} \cong 260$ mA h g^{-1} are provided on the second study in a BiF_3|KHF_2/propylene carbonate (PC)|Pb cell, for which the discharge cut-off voltage is expanded to −0.1 V *vs.* Pb^{2+}/Pb.[17] *Ex situ* X-ray diffraction (XRD) and X-ray photoelectron spectroscopy were measured only for the positive electrode, to conclude the redox reactions between the two electrodes.[16,17]

Toyota Central Research & Development Laboratories, Inc., Yokomichi 41–1, Nagakute, Aichi 480–1192, Japan. E-mail: e4777@mosk.tytlabs.co.jp

† Electronic supplementary information (ESI) available: photographs and schematic structure of the hermetically sealed cell, LSV curve of the Pt|TEAF/PC|Pt cell, full-2θ range XRD patterns at I, D, and C, lattice parameters at I, D, and C, full-2θ range XRD patterns at D(10) and C(10), lattice parameters at D(10) and C(10), Pb(111)/PbF_2(111) ratios in Fig. 2(c), BSE image of the Pb at D(10), BSE image and EDX spectra at C(10), results of the *Q*-limited cycle tests, BSE image and EDX mappings at C(*rcv*), Pb(111)/PbF_2(111) ratios in Fig. 3(c), and XRD pattern of *a*-Pb. See DOI: https://doi.org/10.1039/d2ra05753k

The question then arises whether F^- ions move back and forth between the BiF_3 (positive) and Pb (negative) phases through the liquid-electrolytes. This is because a large amount of the liquid electrolytes in the beaker-type full-cell can supply F^- ions to both electrodes. Furthermore, electrode materials in FIBs easily dissolve into liquid-electrolytes during the discharge and charge reactions,[17,19,25,26] adding to Q_{cha} and Q_{dis} as an extra electric charge. In this sense, a reversible movement of F^- ions between the two electrodes, *i.e.*, reversible redox reaction as that for LIBs, has not been confirmed yet for liquid-electrolyte-type FIBs. Another drawback using the beaker-type full-cell is to diminish the W_{vol} of FIBs, which is one of motivations for pursuing FIBs.

Considering above situation, it is crucial to confirm that a reversible redox reaction occurs in FIBs in a conventional (full-) cell assembly as it does in LIBs.[1,2] This task is essential for further developments and implementation of FIBs, although such a fundamental approach for establishing FIB chemistry seems to have been overlooked in previous FIB studies.[16–26] Therefore, in this study, we fabricated an FIB using a hermetically sealed cell that has been utilized in LIB studies (Fig. S1†). We then examined structural and compositional variations in the electrodes for both positive and negative electrodes by *ex situ* XRD and energy dispersive X-ray (EDX) analyses. BiF_3 and Pb, the most representative electrodes for which redox reactions have been confirmed in half-cells, were selected as positive and negative electrodes.[18–26] We also chose 0.1 M tetraethylammonium fluoride (TEAF) dissolved in PC as a liquid electrolyte (TEAF/PC). TEAF is composed of tetraalkylammonium cations and has a molecular structure similar to those of other previously investigated fluoride salts, such as tetramethylammonium fluoride (TMAF).[19] Consequently, we found that the movement of F^- ions between the BF_3 and Pb electrodes through the TEAF/PC electrolyte is reversible.

Experimental

The positive electrode consisted of 80 wt% BiF_3 powder (Sigma-Aldrich), 10 wt% carbon black (CB, TB5500; Tokai Carbon), and 10 wt% polytetrafluoroethylene (PTFE, F-104; Daikin). For the negative electrode, we used three different types of Pb: Pb plate (Pb-plate, Nilaco), as-received Pb powder (*rcv*-Pb, Kojyundo Chemical Laboratory), and annealed Pb powder (*a*-Pb). To prepare *a*-Pb, *rcv*-Pb was heated at 150 °C for 1 h in a high-frequency induction heating furnace equipped with an Ar-filled glovebox. The Pb-plate was used by itself as a negative electrode. Two negative electrodes were also prepared from powders, and each consisted of a mixture of 80 wt% *rcv*-Pb (or *a*-Pb), 10 wt% CB, and 10 wt% PTFE. The diameters of the positive and negative electrodes were 14 and 16 mm, respectively, and all three electrodes were 200 μm thick. TMAF and TEAF were provided by Sigma-Aldrich; however, we used only TEAF because TMAF was difficult to dissolve into PC (Kishida Chemical). To clarify the voltage window of the TEAF/PC electrolyte (0.1 M), linear sweep voltammetry (LSV, IVIUMSTAT; Hokuto Denko) was conducted at a scan rate of 1 mV s^{-1} and 25 °C using Pt electrodes.

Fig. S1† shows photographs and the schematic structure of the hermetically sealed cell. This two-electrode-type cell is typical for LIBs,[27] but as far as we concerned, it has never been used for liquid-electrolyte-type FIBs. A porous polyethylene film with a thickness of 25 μm (E25MMS; Tonen Chemical) was inserted between the positive (60–100 mg) and negative (480 mg for the Pb plate and 80 mg for the *rcv*-Pb and *a*-Pb powders) electrodes, along with 200 μL of the electrolyte. The amount of the TEAF/PC electrolyte per milligram of electrode materials was calculated to be 0.34–1.4 μL mg^{-1}, which is similar to that (= 0.5–1.0 μL mg^{-1}) of commercial LIBs.[28] After being assembled in the Ar-filled glovebox, the cells were operated with a current of 0.02 mA (~13 μA cm^{-2}) at 25 °C in the range of 0.1–1.2 (or 0.0–1.1 V). We also performed capacity (Q)-limited cycling tests up to a Q of 10, 20 and 30 mA h g^{-1}.

Ex situ XRD was conducted with a Cu-K*a* radiation in the range of 2θ = 10–70°. The lattice parameters were determined by the Cohen method[29] using at least five diffraction lines. The morphologies and compositions were investigated by scanning electron microscopy (SEM; SU3500, Hitachi High-Technologies) and EDX analyses.

Results and discussion

According to the LSV curve shown in Fig. S2,† the voltage window of the TEAF/PC electrolyte was approximately −1 V to +1 V between the Pt electrodes, which is enough for examining electrochemical reactivities of FIBs. Fig. 1(a) shows the discharge and charge curves of the BiF_3|TEAF/PC|Pb-plate cell. The specific Q in the horizontal axis was calculated based on the weight of the BiF_3 sample. The open-circuit voltage was 1.07 V in the freshly fabricated state (= initial state, I). The cell voltage (E) rapidly dropped to ~0.18 V at the beginning of the discharge reaction and then reached a voltage plateau at ~0.29 V, which was higher and flatter than those in previous studies.[16,17] This flat E is characteristic of a two-phase reaction in which E does not obey a simple Nernst equation.[30] Specifically, the discharge reaction can be represented as

$$BiF_3 + 3xe^- \rightarrow (1 - x)BiF_3 + xBi + 3xF^- \quad (1)$$

for the positive electrode and

$$3/2Pb + 3xF^- \rightarrow 3/2(1 - x)Pb + 3x/2PbF_2 + 3xe^- \quad (2)$$

for the negative electrode. As shown in Fig. 1(b), (c), S3(a), and (b),† diffraction lines originated from the Bi and PbF_2 phases are clearly observed in the discharged state at 0.1 V (D). The XRD patterns in Fig. S3(a) and (b),† which provide full-2θ range of 10−70°, are essentially same with those in Fig. 1(b) and (c), respectively. The diffraction lines from the orthorhombic BiF_3 (*o*-BiF_3) phase almost disappear at D, although *o*-BiF_3 and cubic BiF_3 (*c*-BiF_3) phases coexist at I.[31] Abe and co-workers also reported the difference in the electrochemical reactivities between *o*-BiF_3 and *c*-BiF_3, which is attributed to differences in the rate of defluorination between *o*-BiF_3 and *c*-BiF_3.[32] The Bi phase crystallizes into a rhombohedral phase, whereas initial Pb sample

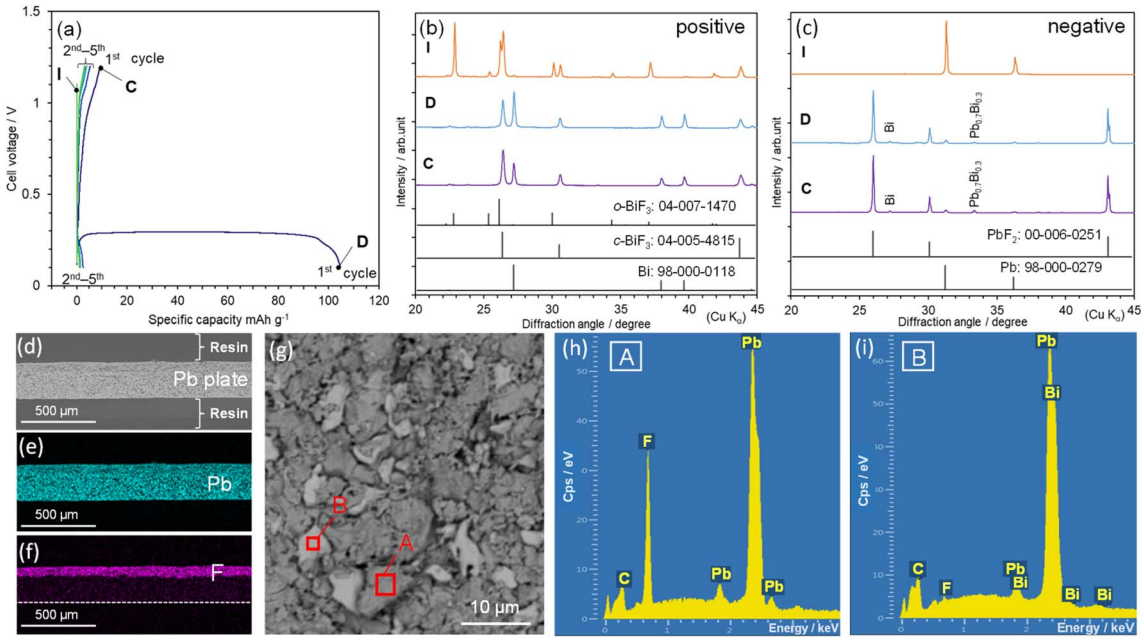

Fig. 1 (a) Discharge and charge curves of the BiF_3|TEAF/PC|Pb-plate cell. *Ex situ* XRD patterns recorded from the (b) BiF_3 and (c) Pb-plate electrodes at various states in (a): initial (I), discharged to 0.1 V (D), and charged to 1.2 V (C). Cross-sectional (d) BSE image and EDX mappings showing (e) Pb and (f) F in the Pb-plate electrode at D. (g) BSE image of the surface of the Pb-plate electrode at D. EDX spectra from areas (h) A and (i) B in (g).

and PbF_2 phase are in a cubic phase. The XRD patterns of *o*-BiF_3, *c*-BiF_3, Bi, PbF_2, Pb are shown in the bottom of Fig. 1(b) and (c) and their lattice parameters are listed in Table S1.†

Because a Q_{dis} of ~105 mA h g^{-1} was obtained at the first cycle, the value of x was calculated to be ~0.35 based on the theoretical Q described in eqn (1) (= 302.3 mA h g^{-1}). However, the subsequent Q_{cha} was less than 10 mA h g^{-1} [Fig. 1(a)]. This extremely irreversible redox reaction can also be understood by the unchanged XRD pattern in the charge state at 1.2 V (C) [Fig. 1(c)]. The origins of this irreversibility are currently unclear, but SEM-EDX analyses at D reveal an inhomogeneous distribution of F^- ions and the dissolution of Bi^{3+} ions into the TEAF/PC electrolyte [Fig. 1(d)–(i)]. According to the back-scattered electron (BSE) images and EDX spectra illustrated in Fig. 1(d)–(f), F atoms penetrate to a depth of ~70 μm, but they are inhomogeneously distributed on the surface. Furthermore, Bi atoms appear in area B at a Pb/Bi ratio of 0.9/0.1, indicating the dissolution of Bi^{3+} ions and decomposition of the TEAF/PC electrolyte. Such an inhomogeneous distribution of F^- ions and the existence of metallic Bi (and/or Pb_yBi_{1-y}) unavoidably decrease the reversibility of the redox reaction. In contrast to that in a beaker-type cell, which contains an excess of electrolyte,[16–26] the electrolyte decomposition in the hermetically sealed cell severely degrades the reversibility of the redox reaction. Fig. 1(c) presents the XRD patterns recorded at points D and C in Fig. 1(a), which confirm the existence of metallic Bi and Pb_yBi_{1-y} in the Pb-plate electrode, although the y value is estimated to be 0.7 from the diffraction angle of ~33.4°.[33]

To suppress the electrolyte decomposition and the formation of metallic Bi and Pb_yBi_{1-y}, we performed Q-limited cycling tests, as shown in Fig. 2(a). One plateau at ~0.27 V appeared during the discharge reaction, and two plateaus occurred at ~0.37 and 0.96 V during the charge reaction. Steady cycling performance appeared at Q = 10 mA h g^{-1}, except for the increase in E at the end of the charge reaction. This increase in E is originated from the distribution and thickness of the PbF_2 phase, as discussed later. Fig. 2(b) shows the *ex situ* XRD patterns of the BiF_3 electrode at Q_{dis} = 10 mA h g^{-1} [D(10)] and Q_{cha} = 10 mA h g^{-1} [C(10)], and Fig. S4(a)† shows their full-2θ range XRD patterns. Diffraction lines from the Bi phase are observed at ~27.2°, 38.2°, and 39.8° at D(10), whereas these diffraction lines have almost disappeared at C(10), indicating the reversible reaction of eqn (1) [Fig. 2(b)]. The diffraction lines from the *o*-BiF_3 phase are weakened at D(10), indicating the preferential reduction of the *o*-BiF_3 phase above ~0.2 V.

For the Q-limited cycle test, the reversible reaction of eqn (2) was verified by the *ex situ* XRD patterns of the Pb-plate electrode, as shown in Fig. 2(c) and S4(b).† The diffraction lines from metallic Bi and Pb_yBi_{1-y} are barely observed at either D(10) or C(10), whereas those from the PbF_2 phase appear at ~26.0°, 30.1°, and 43.1°. Table S2† summarizes the lattice parameters of the BiF_3, Bi, Pb, and PbF_2 phases. Evidently, the Pb(111)/PbF_2(111) ratio increases from 0.24 at D(10) to 0.39 at C(10), where diffraction lines for the Pb(111) and PbF_2(111) planes occur at 31.3° and 26.0°, respectively (Fig. S5†). Moreover, BSE image at D(10) indicates a formation of PbF_2 phase on the Pb plate, while SEM-EDX analyses at C(10) confirm the defluorination of PbF_2 on the surface (Fig. S6 and S7†). These results indicate that Pb was oxidized to PbF_2 during discharging and then PbF_2 was reduced to Pb during charging. Hence,

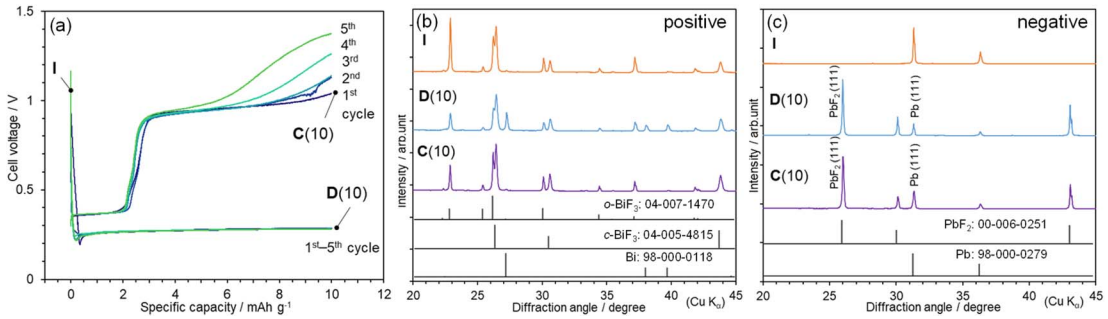

Fig. 2 (a) Q-limited discharge and charge curves of the BiF_3|TEAF/PC|Pb-plate cell when $Q = 10$ mA h g^{-1}. *Ex situ* XRD patterns recorded from the (b) BiF_3 and (c) Pb-plate electrodes at various states in (a): initial (I), $Q_{dis} = 10$ mA h g^{-1} [D(10)], and $Q_{cha} = 10$ mA h g^{-1} [C(10)].

combining eqn (1) and (2), the overall redox reaction of the BiF_3|TEAF/PC|Pb-plate cell can be described by

$$BiF_3 + 3/2Pb \leftrightarrow (1 - x)BiF_3 + xBi + 3/2(1 - x)Pb + 3x/2PbF_2 (3)$$

although x is limited to ~0.033.

The Q values in the Q-limited cycle test were increased to 20 and 30 mA h g^{-1}. As shown in Fig. S8(a),† steady cycling performance is also attained at $Q = 20$ mA h g^{-1}, enlarging the reversible x value in eqn (3) by two times (≅ 0.066). However, at $Q = 30$ mA h g^{-1}, E rapidly drops to ~0.6 V from above 1 V during the charge reaction, indicating the presence of other side reactions [Fig. S8(b)†]. Besides the dissolution of electrodes[17,19,25,26] and/or decomposition of liquid electrolytes that have been pointed out for FIBs, the distribution and thickness of the PbF_2 phase are thought to affect the reduction to Pb at above 1 V. As understood by the BSE images, the PbF_2 layer with a thickness of ~70 μm covered with the Pb plate [Fig. 1(f)], while the non-uniformed PbF_2 islands with a size of ~30 μm partially locates on the Pb plate (Fig. S6†). The partial distribution and thin layer of the PbF_2 phase maintain the electrical conduction between PbF_2 and Pb (or current collector), offering reversible redox reactions.

Here, we wish to verify the redox reaction by comparing the magnitude of observed Q with the amount of the electrolyte used. Because 200 μL of the TEAF/PC electrolyte was injected into one full-cell, the amount of F^- ions in the liquid electrolyte is calculated to be 2×10^{-5} mol, which can deliver to Q of ~0.54 mA h if all the F^- ions in eqn (2) are supplied by the liquid electrolyte. Because Q of 20 mA h g^{-1} corresponds to 1.56 mA h based on the weight of the BiF_3 sample, the reversible movement of F^- ions between the two electrodes, *i.e.*, reversible redox reaction is confirmed.

As reported previously,[7–26] the rechargeable Q values for liquid-electrolyte-type FIBs are somewhat lower than those for all-solid-state FIBs. In this study, Q_{cha} at the first cycle was only ~9 mA h g^{-1} when the discharge cut-off voltage was set to 0.1 V [Fig. 1(a)]. One strategy for raising Q_{cha} is to increase the active surface area involved in the redox reaction. Konishi *et al.* demonstrated that compositing PbF_2 and carbon *via* ball milling increased the specific Q of the resulting PbF_2 electrodes.[24] We thus replaced the Pb-plate with *rcv*-Pb or *a*-Pb as the negative electrode.

Fig. 3(a) shows the discharge and charge curves of the BiF_3|TEAF/PC|*rcv*-Pb cell at the first cycle, where the average particle size of the *rcv*-Pb powder is ~200 μm [Fig. S9(a)†]. The E during the discharge reaction is almost constant at ~0.29 V until ~100 mA h g^{-1}, except for a drop to ~0 V at Q_{dis} < 10 mA h g^{-1}. The Q_{dis} and Q_{cha} values reach 110 and 60 mA h g^{-1}, respectively, yielding a high reversibility of ~55% compared to that (≅ 0.09%) for the BiF_3|TEAF/PC|Pb-plate cell. Note that it took approximately two (one) weeks to complete the discharge (charge) reaction, corresponding to C-rate of C/360 (C/180). This C-rate is significantly lower than those for previous FIB studies using solid-state electrolytes[7] or liquid electrolytes,[17] indicating

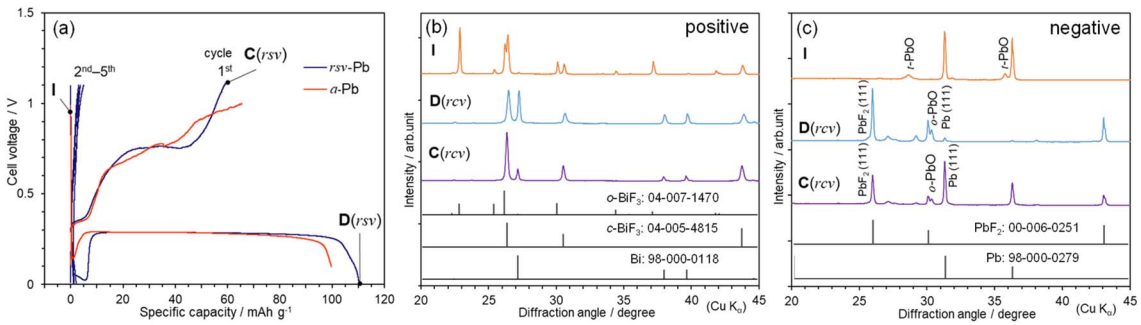

Fig. 3 (a) Discharge and charge curves of the BiF_3|TEAF/PC|*rcv*-Pb and BiF_3|TEAF/PC|*a*-Pb cells. *Ex situ* XRD patterns recorded from the (b) BiF_3 and (c) *rcv*-Pb electrodes in the BiF_3|TEAF/PC|*rcv*-Pb cell at various states in (a): initial (I), discharged to 0 V [D(*rcv*)], and charged to 1.1 V [C(*rcv*)].

that the cell was maintained under a severe condition for a long time. Fig. 3(b) and (c) show *ex situ* XRD patterns of the BiF_3 and *rcv*-Pb electrodes, respectively, at I, discharged down to 0 V [D(*rcv*)] and charged up to 1.1 V [C(*rcv*)]. Bi and PbF_2 phases are produced at D(*rcv*), but the diffraction lines from these phases are weakened at C(*rcv*). The *o*-BiF_3 phase almost disappears at D(*rcv*) and never appear at C(*rcv*), as in the case for the BiF_3-|TEAF/PC|Pb-plate cell when *E* was discharged to 0.1 V. The Pb(111)/PbF_2(111) ratio increases significantly from 0.06 at D(*rcv*) to 1.32 at C(*rcv*) (Fig. S10†), being consistent with the result that *rcv*-Pb indicates a higher reversibility than Pb plate. Additionally, the EDX mappings of Pb and F at C(*rcv*) reveal that the surface of the *rcv*-Pb powder is defluorinated during the charge reaction [Fig. S9(b) and (c)†].

We performed an extended cycle test up to five cycles for the BiF_3|TEAF/PC|*rcv*-Pb cell and illustrate corresponding discharge and charge curves in Fig. 3(a). The Q_{dis} and Q_{cha} values for the subsequent cycles rapidly decrease to ~5 mA h g^{-1}, indicating a similar cycle performance to the BiF_3|TEAF/PC|Pb-plate cell, shown in Fig. 1(a). For the Bi|MPPF + TMPA-TFSA|PbF_2-deposited Pb cell, Q_{dis} decreases from 0.17 mA h to 0.01 mA h after five cycles.[16] In contrast, FIBs using solid electrolytes exhibit a relatively stable cycle performance;[7] for instance, Q_{dis} of 50–60 mA h g^{-1} is maintained up to ten cycles for the BiF_3|$BaSnF_4$|Zn cell.[34] These results indicate difficulties in the improvement of cycle performance of liquid-electrolyte-type FIBs. Further developments such as stabilization of liquid electrolytes are encouraged.

Finally, we attempted to diminish the drop in *E* at Q_{dis} < 10 mA h g^{-1}. As shown in Fig. 3(c), *rcv*-Pb contains a small amount of a tetragonal PbO (*t*-PbO) as an impurity at I, which transforms into an orthorhombic PbO (*o*-PbO) phase at D(*rcv*). Next, we prepared a cell using *a*-Pb, which was produced by annealing *rcv*-Pb under an Ar atmosphere, and we examined the discharge profile. As expected, the drop in *E* was mitigated for the BiF_3-|TEAF/PC|*a*-Pb cell, indicating the involvement of oxygen in the redox reaction [Fig. 3(a)]. The *ex situ* XRD pattern after the first cycle (Fig. S11†) also confirms the absence of the PbO phases.

Conclusions

We examined reaction mechanisms for three types of BiF_3-|TEAF/PC|Pb cell *via ex situ* XRD and EDX analyses. The BiF_3-|TEAF/PC|Pb-plate cell exhibited a flat operating voltage at ~0.29 V during the discharge reaction with a Q_{dis} of 105 mA h g^{-1}. The electrochemical reaction was reversible in the *Q*-limited cycle test less than 20 mA h g^{-1}. The Bi and PbF_2 phases were formed at D(10), while the Pb(111)/PbF_2(111) ratio increased to 0.39 at C(10). Combining the SEM-EDX results at D(10) and C(10), we confirmed the reversible movement of F^- ions between the BiF_3 and Pb electrodes, *i.e.*, redox rection in the liquid-electrolyte-type FIB. We also successfully improved the reversibility of the redox reaction at the first cycle by replacing the Pb plate with *rcv*-Pb or *a*-Pb powder. Specifically, approximately ~55% of the reversibility was attained for the BiF_3|TEAF/PC|*rcv*-Pb cell, while the drop in *E* at Q_{dis} < 10 mA h g^{-1} was mitigated for the BiF_3|TEAF/PC|*a*-Pb cell. These improvements owed to the increase in the active surface area of the Pb electrode without the PbO impurity.

Liquid-electrolyte-type FIBs are saddled with a mountain of issues such as low Q_{dis} (or Q_{cha}) and poor cycle performance, compared to those for LIBs. However, as far as we concerned, this is the first repot that confirms the reversible redox reaction in the liquid-electrolyte-type FIB using a conventional full-cell assembly. Because this type of cell assembly is essential for maximizing the advantages of FIBs, the obtained results shed light on the further development of FIBs.

Author contributions

RY: conceptualization, data curation, writing – original draft. TS: conceptualization. SM: data curation. KM: formal analysis, writing – review & editing, supervision.

Conflicts of interest

There are no conflicts to declare.

Acknowledgements

We are grateful to Dr Nobuko Ohba of TCRDL for the fruitful discussion on the open-circuit voltage of the freshly fabricated cells.

Notes and references

1 T. Ohzuku and A. Ueda, *Solid State Ionics*, 1994, **69**, 201.
2 J. B. Goodenough and K. S. Park, *J. Am. Chem. Soc.*, 2013, **135**, 1167.
3 M. Anji Reddy and M. Fichtner, *J. Mater. Chem.*, 2011, **21**, 17059.
4 F. Gschwind, G. Rodriguez-Garcia, D. J. S. Sandbeck, A. Gross, M. Weil, M. Fichtner and N. Hörmann, *J. Fluorine Chem.*, 2016, **182**, 76.
5 F. Gschwind, Z. Zao-Karger and M. Fichtner, *J. Mater. Chem. A*, 2014, **2**, 1214.
6 F. Gschwind and J. Bastien, *J. Mater. Chem. A*, 2015, **3**, 5628.
7 M. A. Nowroozi, I. Mohammad, P. Molaiyan, K. Wissel, A. R. Munnangi and O. Clemens, *J. Mater. Chem. A*, 2021, **9**, 5980.
8 C. Rongeat, M. Anji Reddy, T. Diemant, R. J. Behm and M. Fichtner, *J. Mater. Chem. A*, 2014, **2**, 20861.
9 D. T. Thieu, M. H. Fawey, H. Bhatia, T. Diemant, V. S. K. Chakravadhanula, R. J. Behm, C. Kübel and M. Fichtner, *Adv. Funct. Mater.*, 2017, **27**, 1701051.
10 M. A. Nowroozi, K. Wissel, M. Donzelli, N. Hosseinpourkahvaz, S. Plana-Ruiz, U. Kolb, R. Schoch, M. Bauer, A. M. Malik, J. Rohrer, S. Ivlev, F. Kraus and O. Clemens, *Commun. Mater.*, 2020, **1**, 27.
11 I. Mohammad, R. Witter, M. Fichtner and M. Anji Reddy, *ACS Appl. Energy Mater.*, 2018, **1**, 4766.
12 M. Murakami, Y. Morita, M. Yonemura, K. Shimoda, M. Mori, Y. Koyama, T. Kawaguchi, K. Fukuda,

Y. Ishikawa, T. Kamiyama, Y. Uchimoto and Z. Ogumi, *Chem. Mater.*, 2019, **31**, 7704.
13 D. Zhang, T. Yoshinari, K. Yamamoto, Y. Kitaguchi, A. Ochi, K. Nakanishi, H. Miki, S. Nakanishi, H. Iba, T. Watanabe, T. Uchiyama, Y. Orikasa, K. Amezawa and Y. Uchimoto, *ACS Appl. Energy Mater.*, 2021, **4**, 3352.
14 M. Uno, M. Onitsuka, Y. Ito and S. Yoshikado, *Solid State Ionics*, 2005, **176**, 2493.
15 L. Liu, L. Yang, M. Liu, X. Li, D. Shao, K. Luo, X. Wang and Z. Luo, *J. Alloys Compd.*, 2020, **819**, 152983.
16 K. Okazaki, Y. Uchimoto, T. Abe and Z. Ogumi, *ACS Energy Lett.*, 2017, **2**, 1460.
17 S. Kawauchi, H. Nakamoto, R. Takekawa, T. Kobayashi and T. Abe, *ACS Appl. Energy Mater.*, 2022, **5**, 2096.
18 H. Konishi, T. Minato, T. Abe and Z. Ogumi, *J. Electrochem. Soc.*, 2017, **164**, A3702.
19 V. K. Davis, C. M. Bates, K. Omichi, B. M. Savoie, N. Momčilović, Q. Xu, W. J. Wolf, M. A. Webb, K. J. Billings, N. H. Chou, S. Alayoglu, R. K. McKenney, I. M. Darolles, N. G. Nair, A. Hightower, D. Rosenberg, M. Ahmed, C. J. Brooks, T. F. Miller III, R. H. Grubbs and S. C. Jones, *Science*, 2018, **362**, 1144.
20 T. Yamamoto, K. Matsumoto, R. Hagiwara and T. Nohira, *J. Electrochem. Soc.*, 2021, **168**, 040530.
21 H. Konishi, T. Minato, T. Abe and Z. Ogumi, *Chem. Lett.*, 2018, **47**, 1346.
22 H. Konishi, A. C. Kucuk, T. Minato, T. Abe and Z. Ogumi, *J. Electroanal. Chem.*, 2019, **839**, 173.
23 H. Konishi, T. Minato, T. Abe and Z. Ogumi, *J. Phys. Chem. C*, 2019, **123**, 10246.
24 H. Konishi, T. Minato, T. Abe and Z. Ogumi, *Mater. Chem. Phys.*, 2019, **226**, 1.
25 H. Konishi, T. Minato, T. Abe and Z. Ogumi, *J. Appl. Electrochem.*, 2018, **48**, 1205.
26 T. Yamamoto, K. Matsumoto, R. Hagiwara and T. Nohira, *ACS Appl. Energy Mater.*, 2019, **2**, 6153.
27 Y.-C. Lu, A. N. Mansour, N. Yabuuchi and Y. Shao-Horn, *Chem. Mater.*, 2009, **19**, 4408.
28 K. Mukai, T. Uyama and T. Nonaka, *ACS Appl. Mater. Interfaces*, 2021, **13**, 42791.
29 M. U. Cohen, *Rev. Sci. Instrum.*, 1935, **6**, 68.
30 T. Ohzuku and A. Ueda, *J. Electrochem. Soc.*, 1997, **144**, 2780.
31 M. Kawasaki, H. Kiuchi, K. Shimoda, G. Kano, H. Fujimoto, Z. Ogumi and T. Abe, *J. Electrochem. Soc.*, 2020, **167**, 120518.
32 T. Yamanaka, K. Okazaki, Z. Ogumi and T. Abe, *ACS Appl. Energy Mater.*, 2019, **2**, 8801.
33 M. Murakami, H.-C. W. Huang, J. Angilello and B. L. Gilbert, *J. Appl. Phys.*, 1983, **54**, 738.
34 I. Mohammad, R. Witter, M. Fichtner and M. A. Reddy, *ACS Appl. Energy Mater.*, 2018, **1**, 4766.